Nanoscale

Accepted Manuscript

This article can be cited before page numbers have been issued, to do this please use: J. Morales-Dalmau, C. Vilches, I. De Miguel, V. Sanz and R. Quidant, *Nanoscale*, 2017, DOI: 10.1039/C7NR06825E.

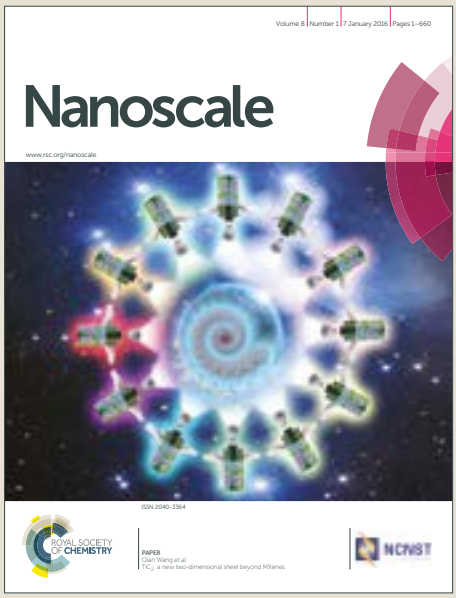

ROYAL SOCIETY OF CHEMISTRY

rsc.li/nanoscale

View Article Online
DOI: 10.1039/C7NR06825E

Optimum morphology of gold nanorods for light-induced hyperthermia

Jordi Morales-Dalmau[1], Clara Vilches[1], Ignacio de Migue1[1], Vanesa Sanz[1], Romain Quidant[1,2].*

1. ICFO - Institut de Ciències Fotòniques, the Barcelona Institute of Science and Technology, 08860 Barcelona, Spain.

2. ICREA - Institució Catalana de Recerca i Estudis Avançats, 08010 Barcelona, Spain.

KEYWORDS: gold nanorods, optimization, thermoplasmonics, hyperthermia, nanomedicine.

ABSTRACT:

Owing to their unique chemical and physical properties, colloidal gold nanoparticles have prompted a wide variety of biocompatible nano-agents for cancer imaging, diagnosis and treatment. In this context, biofunctionalized gold nanorods (AuNRs) are promising candidates for light-induced hyperthermia, to cause local and selective damage in malignant tissue. Yet, the efficacy of AuNR-based hyperthermia is highly dependent on several experimental parameters; in particular, the AuNR morphology strongly affects both physical and biological involved processes. In the present work, we systematically study the influence of different structural parameters like the AuNR aspect ratio, length and molecular weight on *in vitro* cytotoxicity, cellular uptake and heat generation efficiency. Our results enable us to identify the optimum AuNR morphology to be used for *in vivo* hyperthermia treatment.

View Article Online
DOI: 10.1039/C7NR06825E

INTRODUCTION

Beyond the unique optical properties arising from nanoscale matter confinement, there is a growing interest around the photothermal properties of absorbing nanoparticles and their application to heat management[1–6]. Indeed, efficient photothermal nanosources like carbon nanotubes[7,8], graphene oxide flakes[9–11] and metallic nanostructures[12,13] offer great opportunities to remotely control heat generation on the nanometer scale with unprecedented heating/cooling kinetics[14–17]. In this context, noble metal nanostructures, featuring enhanced absorption at their Localized Surface Plasmon Resonances (LSPR), have so far received most attention and already found applications in nanomedicine[18–21]. In particular, colloidal gold nanorods (AuNRs) have shown to be efficient and flexible agents for local and targeted tissue ablation[18,22–29]. The prevalence of AuNRs is not only explained by their tunable photothermal properties throughout the visible to near infra-red wavelength range; it is also due to their high biocompatibility, adaptable surface chemistry and possible large scale production[30–32]. So far, only few studies have investigated the influence of AuNR structural parameters[13,33,34] on their performance as hyperthermia agents. Other investigations[13,33] calculated numerically the influence of the AuNRs aspect ratio on their photothermal performance. More recently, MacKey *et al* reported on a first experimental study, comparing the photothermal properties of three types of AuNR and their capability to induce *in vitro* cell necrosis[34]. Yet, none of these prior reports accounted for the influence of the AuNRs morphology on the involved cell biology, which is of pivotal importance in plasmon-based hyperthermia.

Here we present, for the first time to our knowledge, an exhaustive study accounting for heating performance, cell uptake and toxicity that enables us to identify the optimum AuNR morphology for *in vivo* local hyperthermia treatment.

View Article Online
DOI: 10.1039/C7NR06825E

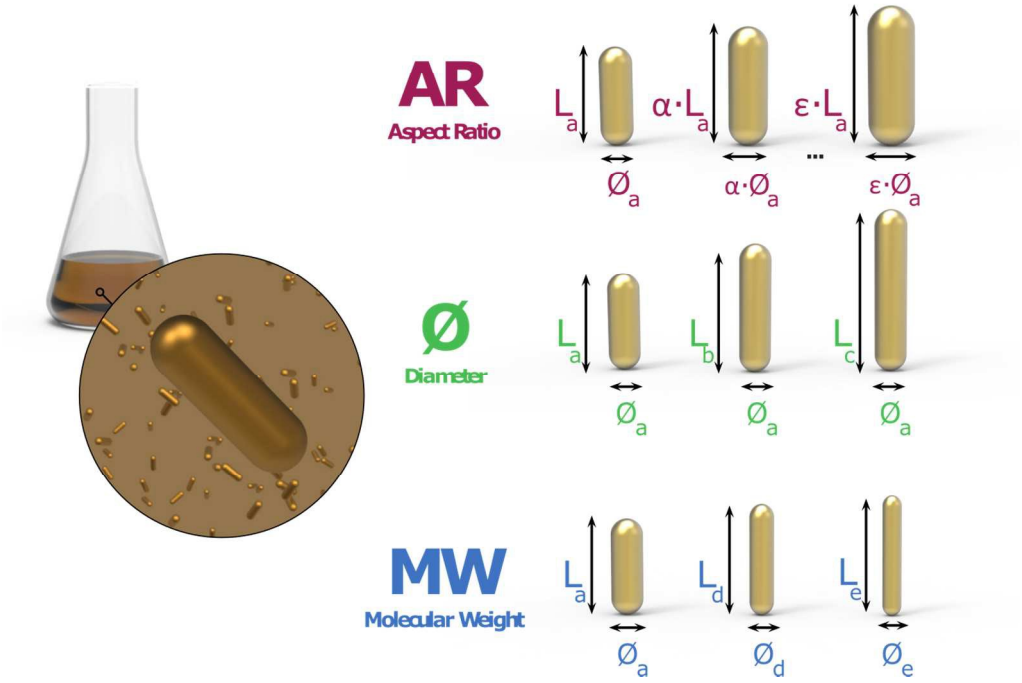

Figure 1. Sketch of the three groups of AuNRs under study. L and ϕ are length and diameter of the AuNRs, respectively. In the first group (in red), AuNRs have fixed aspect ratio (AR=L/ϕ), the second group (in green) is formed by AuNRs with fixed diameter (ϕ) while the AuNRs of the third group (in blue) feature fixed molecular weight (MW). The detailed geometrical parameters of each of the 10 AuNR samples are gathered in **Table 1**.

EXPERIMENTAL

GOLD NANORODS SYNTHESIS

All AuNR suspensions were manufactured in-house in cetyl trimethyl ammonium bromide (CTAB, Sigma-Aldrich) solution by using a slightly modified seed-mediated method[32,35] and maintained at 31ºC. Diameter and length of the AuNRs are controlled following the protocol described in [32] and [35]. While the quantity of gold seed governs the overall volume of the AuNRs, the aspect ratio is determined by the quantity of silver nitrate. Three subgroups of

View Article Online
DOI: 10.1039/C7NR06825E

AuNRs were studied and are summarized in **Figure 1** and **Table 1**. For each solution, size dispersion was estimated to 15% by systematic transmission electron microscopy (TEM) measurements on about one hundred specimens (**Figure S2**). Length and diameter correspond to the central value of the distribution diagram. In general, it has been shown that the aspect ratio (AR), defined as the length to diameter ratio, determines the position of the LSPR[13]. The first subgroup was composed of six different AuNRs with same AR, and therefore same LSPR but different molecular weight (MW). The second subgroup included three AuNRs with fixed diameter but different lengths, and thus, different LSPR and different MW. The third subgroup was formed by three sets of AuNRs with same MW but different AR, and consequently, different LSPR.

#	MW (10^6 Da)	ø (nm)	L (nm)	LSPR (nm)	A (cm^{-1})
1	30	10	32	740	1.43
2	52	12	38	750	2.46
3	82	14	45	746	4.46
4	175	18	57	746	7.60
5	364	23	75	744	15.45
6	740	30	92	744	30.90
7	62	12	46	804	3.60
8	72	12	55	865	4.66
9	52	11	44	808	2.94
10	52	10	48	864	3.30

Table 1. Table of the 10 different AuNR suspensions under study at 1 nM. #: Reference number of the suspension; MW: molecular weight in Dalton (10^6 Da); ø: diameter in nm; L: length in nm; LSPR: Central wavelength of the localized surface plasmon resonance peak in nm; A:

View Article Online
DOI: 10.1039/C7NR06825E

absorbance at the LSPR at 1 nM in cm^{-1}. The characterization of AuNR dimensions was performed using transmission electron microscopy (TEM) (**Figure S2**), with estimated length and diameter dispersion of ±15%. Each subgroup of AuNRs is associated to a different colour: red for the subgroup with AuNRs with fixed AR, green for the subgroup of AuNRs with fixed diameter and blue for the subgroup with fixed MW. Suspension #2 was included in all experiments as inter-assay control.

GOLD NANORODS PEGYLATION

AuNR suspensions were centrifuged at 14000 rpm for 10 minutes, at 31ºC, concentrated 10x by removing 90% of supernatant to remove excess of CTAB. Then, polyethylene glycol (PEG, Iris Biotech GmbH, Germany) was added to the AuNR in an optimal concentration for each nanoparticle. During an overnight process, the CTAB chains were exchanged with PEG moieties. The resulting AuNR-PEG solution was filtered (25 mm RC syringe filter, 0.2 µm pore size, Corning Inc., NY, USA) to remove aggregation or impurities, washed twice and diluted with ultra-pure distilled water (MilliQ).

CHARACTERIZATION OF THE GOLD NANORODS

UV-Vis absorption spectra of all AuNR suspensions in MilliQ water were acquired with a microplate reader (Synergy H1, BioTek Instruments, Inc., Vermont, USA). Optical density (OD) spectra were collected from 400 nm to 998 nm in 2 nm steps, using 96 well plates (polystyrene, clear, flat bottom, Nunc MicroWell, Thermo Fisher Scientific) with 0.69 cm path length (for a final volume of 250 µL). Water spectrum subtraction and triplicates were done for each sample. AuNRs concentration was determined as $c = OD/(l \cdot \epsilon)$, where c (mol/L) is the molar

View Article Online
DOI: 10.1039/C7NR06825E

concentration, OD (a.u.) is the optical density, l (cm) is the path length and ε (1/(cm·mol/L)) is the molar extinction coefficient.

CELL TYPE AND SAMPLE PREPARATION

A-549 (human lung epithelial carcinoma, ATCC CCL-185) and 786-O (human renal clear cell adenocarcinoma, ATCC CRL-1932) cell lines were cultured in Dulbecco's Modified Eagle Medium (DMEM) and Roswell Park Memorial Institute (RPMI) 1640 media, respectively, supplemented with 10% fetal bovine serum (FBS) and maintained at 37ºC and 5% CO_2. Passages were done before cultured flasks reached 80% confluency.

For cytotoxicity and uptake experiments, 5000 cells per well were seeded in 96 well plates (flat bottom, Corning Inc., NY, USA) and let grown for two days. Eventually, each well contained 20000 cells before incubation with AuNR-PEG. In all cases, 100 µL of AuNR-PEG diluted in appropriate culture medium without FBS were added to each well.

CYTOTOXICITY

Cytotoxicity of selected AuNR-PEG samples was assessed at 1 nM and 3 µg of gold per well. After 24 hours of incubation with AuNR-PEG, 20 µL of 5 mg/mL thiazolyl blue tetrazolium bromide (MTT, M2128, CAS 298-93-1, Sigma-Aldrich) were added to each cell well. Plates were incubated at 37ºC and checked every 30 minutes until visualization of formazan crystal formation (~75-90 min). MTT solution was then carefully removed and cells were homogenized in 150 µL of dimethyl sulfoxide (DMSO) to dissolve formazan crystals. Absorbance was measured at 550 nm on a microplate reader (Synergy H1, BioTek Instruments, Inc., Vermont, USA). All plates included appropriate control alive/dead cells and 16 replicas of each condition.

View Article Online
DOI: 10.1039/C7NR06825E

Cellular viability was calculated by extracting the mean MTT signal of the dead control group from the MTT signal from each studied condition and normalizing it with the mean MTT signal from the alive control group.

UPTAKE

Cellular uptake of selected AuNR-PEG was measured in A-549 cells by means of two-photon luminescence (TPL) imaging using a confocal microscope (Leica TCS SP5, Leica Microsystems) coupled to a Kerr lens mode-locked Ti:sapphire laser (Mira900, Coherent with 200 fs pulse duration at a frequency of 80 MHz) tuned at the AuNRs resonance, and 35 mJ of average energy. For cellular uptake study, different AuNR-PEG concentrations were prepared as described above in order to add 3 µg of gold per well. Before TPL imaging, the culture medium containing excess of AuNR-PEG was removed from the wells, cells were fixed with 2% paraformaldehyde (PFA) for 15 minutes, washed twice with phosphate-buffered saline (PBS) solution and let in 1% PFA. TPL signal from internalized AuNR-PEG was measured after 2 hours, 6 hours, and 24 hours of incubation with cells. TPL and bright field images from two random positions in the well and triplicates for each type of incubated nanoparticles were acquired (n=6 for each AuNR suspension). The calibration curve of the TPL signal for each type of AuNR-PEG was acquired using a suspension of these AuNR-PEG in water at different molar concentrations (data not shown). Image processing and AuNR uptake quantification was done using ImageJ software. Bright field images were used to demarcate cell boundaries to ensure TPL signal quantification from internalized AuNRs.

HEATING STUDY

View Article Online
DOI: 10.1039/C7NR06825E

To evaluate the heating efficiency of the different AuNRs, 300 μL of each suspension at 0.5 nM (if not specified otherwise) were added to poly(methyl methacrylate) (PMMA) cuvettes with 10 mm path length (Brand 759115, Sigma-Aldrich). Suspensions were illuminated from the top with a 2 cm diameter beam from a tunable Ti:sapphire laser (Mira900, Coherent) in CW mode, adjusted at the LSPR wavelength of each suspension. Changes in suspensions' temperature were recorded with an infrared (IR) camera (A35sc, FLIR) at 15 Hz in a region of interest (ROI) perpendicular to the largest surface of the cuvette. Prior to laser exposure, a baseline of the initial temperature was obtained for 25 seconds; samples were then illuminated during 10 minutes and temperature was recorded for 10 additional minutes after switching off the laser.

The temperature behavior of suspension number #2 (**Table 1**) was further studied under different conditions of laser power (150 mW, 300 mW, 450 mW and 600 mW), with fixed concentration of particles at 0.5 nM (**Figure S1(a)** and **Figure S1(b)**). Additionally, we studied heating of different AuNR concentrations (0.1 nM, 0.17 nM, 0.5 nM and 1 nM) under fixed laser power at 300 mW), at constant exposure time (**Figure S1(c)**).

RESULTS

OPTICAL CHARACTERIZATION OF AuNRs

The absorbance spectra of the ten AuNR suspensions (**Figure 1** and **Table 1**), at a fixed molar concentration per total gram of gold, are shown in **Figure 2**. The measured spectra for the group of AuNRs with fixed AR verifies that the wavelength of the LSPR peak is maintained despite the gold volume increase, in **Figure 2(a)**. For the group of AuNRs with constant diameter, in good agreement with theory[29], the LSPR peak is shifting to larger wavelengths when increasing AR, as shown in **Figure 2(b)**. Less intuitive, in the group of AuNRs with constant MW (fixed quantity

View Article Online
DOI: 10.1039/C7NR06825E

of gold), the maximum absorbance at the LSPR increases with the AR (**Figure 2(c)**). We can argue that longer and thinner nanocylinders leads to larger electronic currents circulating along in their longer axis and, hence, greater Joule effect. Our optical data enable us to validate the quality of our samples and illustrate possible ways of tuning the efficiency of AuNRs to interact and absorb light as other investigations pointed out before[31,36].

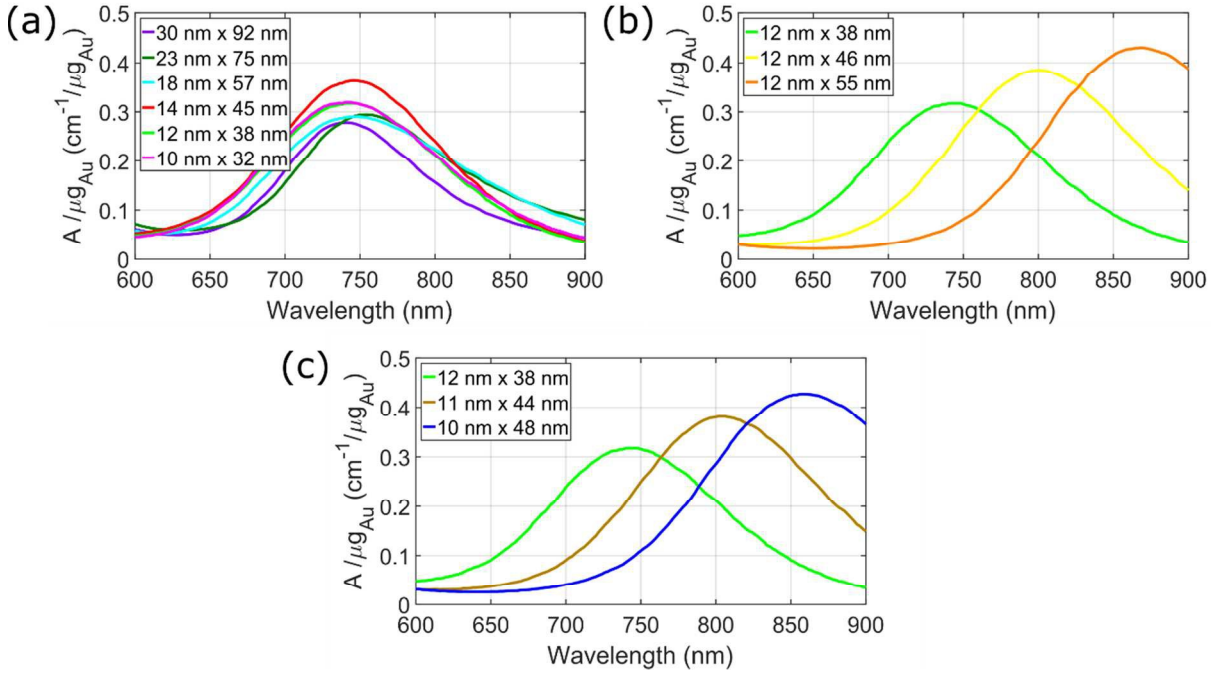

Figure 2. Absorbance (A) spectra of the different AuNR suspensions in $cm^{-1}/\mu g$. (a) AuNR with AR = 3.2 and LSPR centered at ~745 nm (samples #1 to #6 in **Table 1**). (b) AuNR with ϕ = 12 nm and different L (samples #2, #7 and #8 in **Table 1**). (c) AuNR with MW = $52 \cdot 10^6$ and different AR (samples #2, #9 and #10 in **Table 1**).

CYTOTOXICITY

Cytotoxicity was assessed *in vitro* for four types of AuNRs with different diameters but fixed AR (10 nm, 14 nm, 18 nm and 23 nm, in **Figure 3**). Cell viability was analysed in A-549 and 786-O cells, from human lung and renal adenocarcinoma respectively, after 24 hours of incubation with

View Article Online
DOI: 10.1039/C7NR06825E

the AuNRs. At a fixed concentration of 1 nM (**Figure 3**, blue and red dots), cell viability decreased as the diameter of the particle increased, reducing viability down to 15% in those cells incubated with 23 nm diameter AuNRs. Since different nanoparticle sizes result in different quantity of gold at determined molar concentrations, cells were also incubated with AuNR at a fixed concentration of gold (**Figure 3**, green and purple stars). This quantity was set at 3 µg of gold per well as this was the total gold used with the smallest AuNR suspension (10 nm diameter, sample #1 in **Table 1**). Under these conditions, all tested AuNR showed very low cytotoxicity and cell viability was maintained around 85-95% compared to control alive cells. In both studied conditions, fixed concentration and fixed amount of gold, no differences between cell lines were observed. Altogether, it was shown that cell viability was not affected by the size of the nanorods but it was truly determined by the quantity of gold.

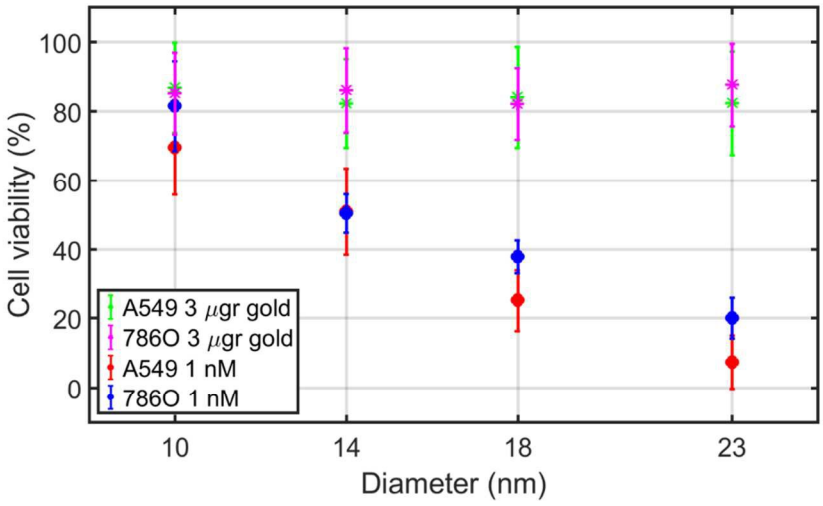

Figure 3. Cell viability after 24 hours of incubation with AuNRs. Cell viability (%) relative to alive control cells is shown for the four tested AuNR suspensions (corresponding to suspension #1, #3, #4 and #5 in **Table 1**) in the A-549 and the 786-O cell lines under different experimental conditions. Error bars show the error propagation of the standard deviation.

View Article Online
DOI: 10.1039/C7NR06825E

UPTAKE

Cellular uptake of AuNRs in A-549 cells after 2 hours, 6 hours and 24 hours incubation times is shown in **Figure 4**. For the four selected AuNR types (10 nm, 14 nm, 18 nm and 23 nm diameter, AuNRs sample #1, #3, #4 and #5 in **Table 1**, respectively), the quantity of gold was fixed at 3 µg of Au in 100 µL of suspension as this amount was previously demonstrated to be non-toxic (cell viability was above 50% and cells maintained their morphology and activity, shown in **Figure 3**). This fixed amount of gold corresponds to concentrations of 1 nM, 0.365 nM, 0.171 nM and 0.08 nM for 10 nm, 14 nm, 18 nm and 23 nm diameter AuNRs, respectively. Maximal cellular uptake was obtained at 24 hours of incubation. Smaller nanoparticles (10 nm) showed higher uptake at all analyzed time points, with 3.5-fold, 5-fold and 13-fold greater internalization compared to 14 nm, 18 nm and 23 nm AuNRs, respectively.

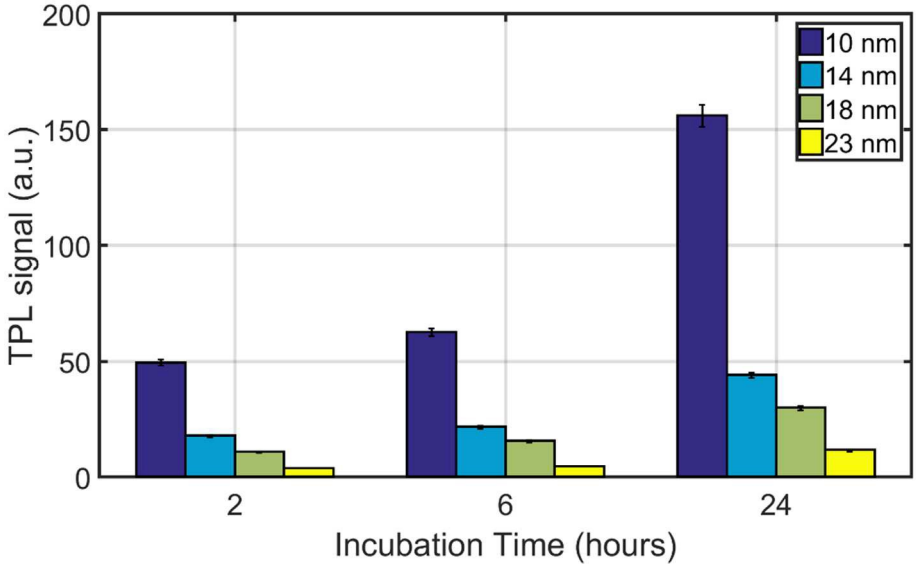

Figure 4. Cellular uptake of AuNRs. Two photon luminescence signal (TPL, in arbitrary units) of different AuNRs (number #1, #3, #4 and #5 in **Table 1**) was used to quantify the cellular uptake at different incubation times (2 hours, 6 hours and 24 hours). Measurements on known

View Article Online
DOI: 10.1039/C7NR06825E

concentrations of AuNRs were used to calibrate the TPL signal. Error bars show the error propagation of the standard deviation.

HEATING STUDY

Here, we studied how the maximum temperature depends on the number of nanoparticles and also on the total amount of gold in the suspension. This allowed us to understand the dependence of heat generation from AuNRs with different sizes and shapes (**Figure 5**). The maximum temperature increase of the different suspensions with fixed AR divided per the total number of nanoparticles reached a saturation-like plateau for larger AuNRs, in **Figure 5(a)**. The maximum temperature increase per gram of gold of the different suspensions with fixed AR was prominently increased for smaller AuNRs, in **Figure 5(b)**. Similarly, in **Figure 5(c)** and in **Figure 5(d)**, all the three groups are shown together in order to evaluate the maximum temperature increase at a fixed molar concentration and fixed gold content, respectively.

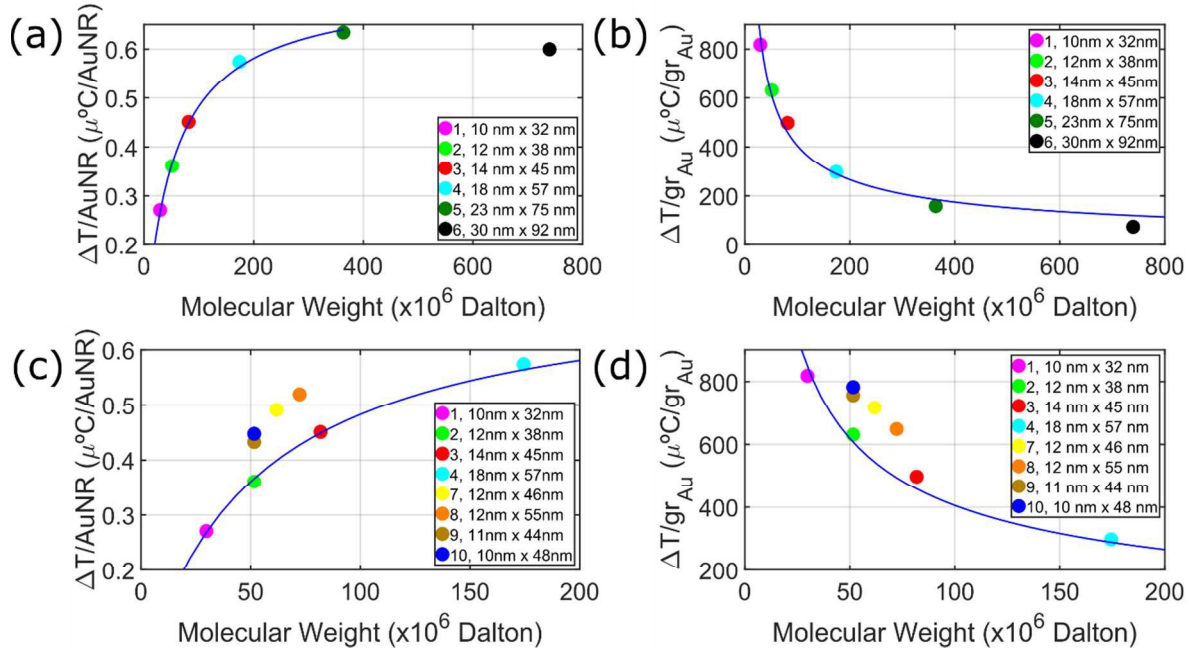

Figure 5. Temperature increase per nanoparticle and per gram of gold for the different suspensions of AuNRs. (a) Maximum temperature increase per nanoparticle as a function of

View Article Online
DOI: 10.1039/C7NR06825E

MW, for the AuNRs in the subgroup with fix AR (number #1-#6 in **Table 1**). (b) Same as (a) per gram of gold (c) Maximum temperature increase per nanoparticle as a function of their MW, for all ten AuNRs used in the experiments. The maximum molecular weight was cut at 200 x10^6 Da (Da = gr/mol). (d) Same as (c) per gram of gold. The MW is cut at 200 x10^6 Da.

DISCUSSION

The data presented in this work enables us to assess the influence of both external (such as power and exposure time of the incoming laser beam) and intrinsic factors (such as morphology and local concentration of AuNRs) on local hyperthermia induced by gold nanoparticles. By studying for the first time, photothermal performance, cellular uptake and toxicity on up to 10 different AuNRs samples, we are able to identify their best morphology towards optimum *in vivo* local hyperthermia treatment.

Optimizing *in vivo* hyperthermia treatment, first requires minimizing intrinsic tissue absorption of the treating light source in order to both reduce damage of healthy tissue and enable a therapeutic effect in further depth. Owing to their different constituents (such as haemoglobin and water), tissue absorption is strongly wavelength-dependent, featuring a transparency window between 650 nm and 950 nm, also known as biological or therapeutic optical window. By choosing AuNRs with the right aspect ratio (AR, from 3 to 5), one can tune their plasmon resonance, and thus their absorption band, into the desired spectral range (**Figure 2(a)** and **Figure 2(c)**). Within this allowed AR range, a second parameter to optimize hyperthermia treatment is to maximize the light-to-heat conversion efficiency of AuNRs and consequently, the absorption contrast between bare tissue and AuNR-decorated tissue. Our data illustrates that, within the set of considered parameters, the photo-heating efficiency of AuNRs saturates with increasing molecular weight (MW) (**Figure 5(a)**). This can be understood by both an increase in

View Article Online
DOI: 10.1039/C7NR06825E

light scattering and the finite penetration of light inside gold (known as skin depth) that eventually translates into lower temperature increase per gram of gold (**Figure 5(b)**). Significantly, smaller AuNRs with LSPR centered in the tissue optical window (around 800 nm) perform better as heat sources than larger AuNRs (**Figure 5(c)** and **Figure 5(d)**).

Cytotoxicity of AuNRs is shown to be independent of the shape of the AuNRs, and only increased with the absolute quantity of gold in the suspension. This is demonstrated in two different cell lines, A-549 cells and 786-O cells, as relevant model for our investigations[37]. Our uptake measurements point out that for a fixed non-cytotoxic gold concentration (3 μg of gold per well in our case), smaller AuNRs are more effectively internalized inside the cell membrane than larger ones. Specific uptake mechanisms were not further studied for these AuNRs, but nanoparticles are likely to follow an endocytosis internalization pathway which favors smaller molecules[38]. Therefore, more AuNRs with smaller diameter could accumulate in the cell without toxic side effects and, thus, maximize local enhancement of photothermal therapy.

Literature shows that *in vivo* toxicity and pharmacokinetics for inorganic AuNRs with hydrodynamic diameter ranging from 10 nm to 100 nm -including biofunctionalization- is not significantly dependent of the AuNR size although they slightly improve for smaller sizes[39,40]. Consequently, our conclusions should mostly remain valid *in vivo*. Nevertheless, other parameters, such as administration route[41], dosage[42], shape[43] or biochemical functionalization[44], might have more influence[40].

Overall, we experimentally demonstrate that AuNRs with a diameter smaller than 12 nm and a LSPR at around 800 nm –such as sample #7 in **Table 1**- are the most promising AuNRs for local hyperthermia. These AuNRs have high cellular uptake, high heating efficiency compared with the ones with the same MW and their LSPR is located in 804 nm, just in the middle of the optical

View Article Online
DOI: 10.1039/C7NR06825E

biological window, where the absorption of the most important chromophores in tissue is minimum.

CONCLUSIONS

In this article we learned that both, cellular uptake of AuNRs and temperature increase under laser irradiation, do not only depend on the volume of the AuNRs, but also on their shape. This information is crucial to optimize the AuNRs morphology for any use of these nanoparticles for *in vivo* treatments. We demonstrate that AuNRs with diameter of about 10 nm and surface plasmon resonance centered at 800 nm have the best potential for future treatments based on photothermal ablation.

AUTHOR INFORMATION

Corresponding Author

*E-mail: Romain.quidant@icfo.eu

ORCID

Romain Quidant: 0000-0001-8995-8976

Notes

The authors declare no competing financial interest.

ACKNOWLEDGEMENTS

We acknowledge the support from Fundació CELLEX Barcelona, the CERCA Programme/ Generalitat de Catalunya and the Spanish Ministry of Economy and Competitiveness, under grants PHOTODEMENTIA, DPI2015-64358-C2-1-R and the 'Severo Ochoa' Programme for

View Article Online
DOI: 10.1039/C7NR06825E

Centres of Excellence in R&D (SEV-2015-0522). The authors would also like to thank Dr. Pascal Berto, Dr. Jon Donner, Dr. Renaud Marty, Miguel Mireles, Prof. Dr. Turgut Durduran and Dr. Alexander Powell and Marc Montagut for useful discussions and assistance.

BIBLIOGRAPHY

(1) Baffou, G.; Quidant, R. Thermo-Plasmonics: Using Metallic Nanostructures as Nano-Sources of Heat. *Laser Photon. Rev.* **2013**, *7*, 171–187.

(2) Novotny, L.; van Hulst, N. Antennas for Light. *Nat Phot.* **2011**, *5*, 83–90.

(3) Punj, D.; Mivelle, M.; Moparthi, S. B.; van Zanten, T. S.; Rigneault, H.; van Hulst, N. F.; Garcia-Parajo, M. F.; Wenger, J. A Plasmonic "antenna-in-Box" platform for Enhanced Single-Molecule Analysis at Micromolar Concentrations. *Nat Nano* **2013**, *8*, 512–516.

(4) Mühlschlegel, P.; Eisler, H.-J.; Martin, O. J. F.; Hecht, B.; Pohl, D. W. Resonant Optical Antennas. *Sci.* **2005**, *308*, 1607–1609.

(5) Bharadwaj, P.; Deutsch, B.; Novotny, L. Optical Antennas. *Adv. Opt. Photonics* **2009**, *1*, 438–483.

(6) Feng, W.; Chen, L.; Qin, M.; Zhou, X.; Zhang, Q.; Miao, Y.; Qiu, K.; Zhang, Y.; He, C. Flower-like PEGylated MoS2 Nanoflakes for near-Infrared Photothermal Cancer Therapy. *Sci. Rep.* **2015**, *5*, 17422.

(7) Kostarelos, K.; Bianco, A.; Prato, M. Promises, Facts and Challenges for Carbon Nanotubes in Imaging and Therapeutics. *Nat Nano* **2009**, *4*, 627–633.

(8) Baloch, K. H.; Voskanian, N.; Bronsgeest, M.; Cumings, J. Remote Joule Heating by a Carbon Nanotube. *Nat Nano* **2012**, *7*, 316–319.

(9) Yang, K.; Zhang, S.; Zhang, G.; Sun, X.; Lee, S. T.; Liu, Z. Graphene in Mice: Ultrahigh in Vivo Tumor Uptake and Efficient Photothermal Therapy. *Nano Lett.* **2010**, *10*, 3318–3323.

(10) Robinson, J. T.; Tabakman, S. M.; Liang, Y.; Wang, H.; Sanchez Casalongue, H.; Vinh, D.; Dai, H. Ultrasmall Reduced Graphene Oxide with High near-Infrared Absorbance for Photothermal Therapy. *J. Am. Chem. Soc.* **2011**, *133*, 6825–6831.

(11) Turcheniuk, K.; Dumych, T.; Bilyy, R.; Turcheniuk, V.; Bouckaert, J.; Vovk, V.; Chopyak, V.; Zaitsev, V.; Mariot, P.; Prevarskaya, N.; *et al.* Plasmonic Photothermal Cancer Therapy with Gold Nanorods/reduced Graphene Oxide Core/shell Nanocomposites. *RSC Adv.* **2016**, *6*, 1600–1610.

(12) Govorov, A. O.; Richardson, H. H. Generating Heat with Metal Nanoparticles. *Rev. Lit. Arts Am.* **2007**, *2*, 30–38.

View Article Online
DOI: 10.1039/C7NR06825E

(13) Baffou, G.; Quidant, R.; Girard, C. Heat Generation in Plasmonic Nanostructures: Influence of Morphology. *Appl. Phys. Lett.* **2009**, *94*, 153103–153109.

(14) Baffou, G.; Quidant, R.; de Abajo, F. J. Nanoscale Control of Optical Heating in Complex Plasmonic Systems. *ACS Nano* **2010**, *4*, 709–716.

(15) Sanchot, A.; Baffou, G.; Marty, R.; Arbouet, A.; Quidant, R.; Girard, C.; Dujardin, E. Plasmonic Nanoparticle Networks for Light and Heat Concentration. *ACS Nano* **2012**, *6*, 3434–3440.

(16) Li, J.; Liu, J.; Chen, C. Remote Control and Modulation of Cellular Events by Plasmonic Gold Nanoparticles: Implications and Opportunities for Biomedical Applications. **2017**.

(17) Baffou, G.; Urena, E. B.; Berto, P.; Monneret, S.; Quidant, R.; Rigneault, H. Deterministic Temperature Shaping Using Plasmonic Nanoparticle Assemblies. *Nanoscale* **2014**, *6*, 8984–8989.

(18) O'Neal, D. P.; Hirsch, L. R.; Halas, N. J.; Payne, J. D.; West, J. L. Photo-Thermal Tumor Ablation in Mice Using near Infrared-Absorbing Nanoparticles. *Cancer Lett.* **2004**, *209*, 171–176.

(19) Bardhan, R.; Lal, S.; Joshi, A.; Halas, N. J. Theranostic Nanoshells: From Probe Design to Imaging and Treatment of Cancer. *Acc. Chem. Res.* **2011**, *44*, 936–946.

(20) Wang, Y.; Black, K. C. L.; Luehmann, H.; Li, W.; Zhang, Y.; Cai, X.; Wan, D.; Al, W. E. T. Comparison Study of Gold Nanohexapods, Nanorods, and Nanocages for Photothermal Cancer Treatment. **2013**, 2068–2077.

(21) Durr, N. J.; Larson, T.; Smith, D. K.; Korgel, B. A.; Sokolov, K.; Ben-Yakar, A. Two-Photon Luminescence Imaging of Cancer Cells Using Molecularly Targeted Gold Nanorods. *Nano Lett.* **2007**, *7*, 941–945.

(22) West, J. L. Nanoshell-Mediated near-Infrared Thermal Therapy of Tumors under Magnetic Resonance Guidance. *PNAS* **2003**, *100*, 13549–13554.

(23) Link, S.; El-Sayed, M. A. Shape and Size Dependence of Radiative, Non-Radiative and Photothermal Properties of Gold Nanocrystals. *Int. Rev. Phys. Chem.* **2000**, *19*, 409–453.

(24) Goodman, A. M.; Cao, Y.; Urban, C.; Neumann, O.; Ayala-Orozco, C.; Knight, M. W.; Joshi, A.; Nordlander, P.; Halas, N. J. The Surprising in Vivo Instability of Near-IR-Absorbing Hollow Au–Ag Nanoshells. *ACS Nano* **2014**, *8*, 3222–3231.

(25) Dickerson, E. B.; Dreaden, E. C.; Huang, X.; El-Sayed, I. H.; Chu, H.; Pushpanketh, S.; McDonald, J. F.; El-Sayed, M. A. Gold Nanorod Assisted near-Infrared Plasmonic Photothermal Therapy (PPTT) of Squamous Cell Carcinoma in Mice. *Cancer Lett.* **2008**, *269*, 57–66.

(26) Huang, X.; El-Sayed, I. H.; Qian, W.; El-Sayed, M. a. Cancer Cell Imaging and Photothermal Therapy in the near-Infrared Region by Using Gold Nanorods. *J. Am. Chem. Soc.* **2006**, *128*, 2115–2120.

View Article Online
DOI: 10.1039/C7NR06825E

(27) Liu, Y. Human Induced Pluripotent Stem Cells for Tumor Targeted Delivery of Gold Nanorods and Enhanced Photothermal Therapy. *ACS Nano* **2016**, *10*, 2375–2385.

(28) Abadeer, N. S.; Murphy, C. J. Recent Progress in Cancer Thermal Therapy Using Gold Nanoparticles. *J. Phys. Chem. C* **2016**, *120*, 4691–4716.

(29) Near, R. D.; Hayden, S. C.; El-Sayed, M. A. Thin to Thick, Short to Long: Spectral Properties of Gold Nanorods by Theoretical Modeling. *J. Phys. Chem. C* **2013**, *117*, 18653–18656.

(30) Weintraub, K. Biomedicine: The New Gold Standard. *Nature* **2013**, *495*, S14–S16.

(31) Chen, H.; Shao, L.; Li, Q.; Wang, J. Gold Nanorods and Their Plasmonic Properties. *Chem. Soc. Rev.* **2013**, *42*, 2679–2724.

(32) Nikoobakht, B.; El-Sayed, M. A. Preparation and Growth Mechanism of Gold Nanorods (NRs) Using Seed-Mediated Growth Method. *Chem. Mater.* **2003**, *15*, 1957–1962.

(33) Kessentini, S.; Barchiesi, D. Quantitative Comparison of Optimized Nanorods, Nanoshells and Hollow Nanospheres for Photothermal Therapy. *Biomed. Opt. Express* **2012**, *3*, 590.

(34) MacKey, M. a.; Ali, M. R. K.; Austin, L. a.; Near, R. D.; El-Sayed, M. a. The Most Effective Gold Nanorod Size for Plasmonic Photothermal Therapy: Theory and in Vitro Experiments. *J. Phys. Chem. B* **2014**, *118*, 1319–1326.

(35) Pérez-Juste, J.; Pastoriza-Santos, I.; Liz-Marzán, L. M.; Mulvaney, P. Gold Nanorods: Synthesis, Characterization and Applications. *Coord. Chem. Rev.* **2005**, *249*, 1870–1901.

(36) Zhu, J. Shape Dependent Full Width at Half Maximum of the Absorption Band in Gold Nanorods. *Phys. Lett. Sect. A Gen. At. Solid State Phys.* **2005**, *339*, 466–471.

(37) Johansson, J.; Mireles, M.; Morales, J.; Farzam, P.; Martínez, M.; Casanovas, O.; Durduran, T. Scanning, Non-Contact, Hybrid Broadband Diffuse Optical Spectroscopy and Diffuse Correlation Spectroscopy System. *Biomed. Opt. Express* **2016**, *7*, 481.

(38) Oh, N.; Park, J. H. Endocytosis and Exocytosis of Nanoparticles in Mammalian Cells. *Int. J. Nanomedicine* **2014**, *9*, 51–63.

(39) Yu, M.; Zheng, J. Clearance Pathways and Tumor Targeting of Imaging Nanoparticles. **2015**, 6655–6674.

(40) Wilhelm, S.; Tavares, A. J.; Dai, Q.; Ohta, S.; Audet, J.; Dvorak, H. F.; Chan, W. C. W. Analysis of Nanoparticle Delivery to Tumours. **2016**.

(41) Bednarski, M.; Dudek, M.; Knutelska, J.; Nowiński, L.; Sapa, J.; Zygmunt, M.; Nowak, G.; Luty-Błocho, M.; Wojnicki, M.; Fitzner, K.; *et al.* The Influence of the Route of Administration of Gold Nanoparticles on Their Tissue Distribution and Basic Biochemical Parameters: In Vivo Studies. *Pharmacol. Reports* **2015**, *67*, 405–409.

(42) Puvanakrishnan, P. In Vivo Tumor Targeting of Gold Nanoparticles: Effect of Particle Type and Dosing Strategy. *Int. J. Nanomedicine* **2012**, 1251.

View Article Online
DOI: 10.1039/C7NR06825E

(43) Truong, N. P.; Whittaker, M. R.; Mak, C. W.; Davis, T. P. The Importance of Nanoparticle Shape in Cancer Drug Delivery. *Expert Opin. Drug Deliv.* **2014**, 1–14.

(44) Akiyama, Y.; Mori, T.; Katayama, Y.; Niidome, T. The Effects of PEG Grafting Level and Injection Dose on Gold Nanorod Biodistribution in the Tumor-Bearing Mice. *J. Control. Release* **2009**, *139*, 81–84.

View Article Online
DOI: 10.1039/C7NR06825E

A systematic study of the influence of gold nanorod morphology on cellular toxicity, uptake and light to heat conversion